Optics and Spectroscopy, 2024, Vol. 132, No. 1

05

Pulsed laser annealing of silicon implanted with manganese ions

© *M.S. Kovalev* [1], *I.M. Podlesnykh* [1,¶], *R.I. Batalov* [2], *N.G. Stsepuro* [1], *S.I. Kudryashov* [1]

[1] Lebedev Physical Institute, Russian Academy of Sciences,
119991 Moscow, Russia
[2] Zavoisky Physical-Technical Institute, FRC „Kazan Scientific Center of RAS",,
420029 Kazan, Russia

[¶] e-mail: i.podlesnykh@lebedev.ru

Received December 11, 2023
Revised January 09, 2024
Accepted January 16, 2024

This work describes a technique for pulsed laser annealing of silicon preliminarily hyperdoped with manganese atoms using ion implantation. Optimal laser annealing regimes were selected which provided the best crystallinity of the samples. In this work the influence of pulsed laser annealing on some optical and structural properties of hyperdoped silicon wafers was also analyzed through studies of Raman spectra, studies of the atomic composition of the material using energy-dispersive X-ray spectroscopy, as well as studies of infrared absorption spectra in the wavenumber range from 700 cm^{-1} to 1300 cm^{-1}.

Keywords: pulsed laser annealing, hyperdoping, ion implantation, silicon, manganese.

DOI: 10.61011/EOS.2024.01.58288.13-24

Introduction

As known, crystalline lightly-doped silicon (Si) is an indirect-band-gap semiconductor with a band gap of $E_g = 1.12$ eV at $T = 300$ K. It has a good capacity of absorbing ultraviolet (UV), visible and near-infrared (IR) radiation (0.4$-$1 μm), but is almost transparent in a more long-wavelength portion of the near- and middle-IR region (1$-$15 μm). Therefore, Si is widely used in optoelectronics as a material for photodiodes with a photosensitivity edge up to approx. 1 μm. Si doping with shallow-level (ionization energy lower than 0.05 eV) p-type (B) or n-type (P, As, Sb) impurities from periodic groups III and V helps provide the required type and conductivity, and this is extensively used in micro- and optoelectronics applications for creation of a wide range of devices. Whilst there is a great demand for enhancement of Si functionality to the near- and middle-IR regions (1$-$10 μm), where narrow-bandgap semiconductors A_3B_5 (InAs, InSb) and CdHgTe, whose treatment technique is low compatible with traditional silicon treatment, are the base materials for optoelectronics.

A promising approach to increasing Si absorption in the 1$-$10 μm range involves Si hyperdoping [1] with deep-level (ionization energy 0.1$-$0.5 eV) impurities such as chalcogens (S, Se, Te) [2,3] or transition and noble metals (Ti, V, Fe, Co, Ni, Ag, Au) [4]. Si hyperdoping means implantation of an impurity in a concentration range above 10^{19} cm^{-3}. Such doping level is considerably higher (by several orders of magnitude) than the equilibrium solubility values of these impurities in Si ($\approx 10^{15} - 10^{16}$ cm^{-3}) and is followed by formation of impurity bands. The presence of impurity bands facilitates absorption of low-energy photons with $E < E_g$(Si). To achieve such high doping levels, non-equilibrium methods are required such as ion implantation and pulsed (femto-, pico- and nanosecond) laser irradiation through fast melt and crystallization processes ($\approx 1-5$ m/s). Rapid development in this research area (Si hyperdoping) has started since the 2000s and to this point promising results have been achieved for high optical absorption level of Si in the 1$-$10 μm range (up to 50%) and for photosensitivity on photodiode structures up to 500 mA/W at the telecommunications wavelengths of 1.31 μm and 1.55 μm.

According to the existing reviews of Si hyperdoping, Ti, V, Fe, Co, Ni are the primary doping impurities from the range of transition $3d$-metals. No studies on Si hyperdoping with manganese (Mn) for optoelectronic applications have been found. The existing literature [5] reports that Mn impurity in Si forms two p-type levels ($E_v + 0.33$ and $E_v + 0.55$ eV). At the same time, Mn impurity in Si is deemed as promising for creation of a ferromagnetic semiconductor [6–9] for spintronics applications. This is covered in a series of studies on Si implantation with high doses of Mn^+ with following fast thermal or laser annealing that reported on the achievement of ferromagnetism at $T > 300$ K [10,11].

Thus, Mn impurity behavior in Si is of research and applied interest both for optoelectronics in terms of development of IR-range (1 $-$ 10 μm) photo-sensitive devices and for spintronics in terms of development of spin injectors. The study employs pulsed laser annealing (PLA) of a n-Si plate implanted with low-energy (40 keV) Mn^+. The effect of PLA on some structural and optical properties of exposed Si:Mn layers will be also addressed.

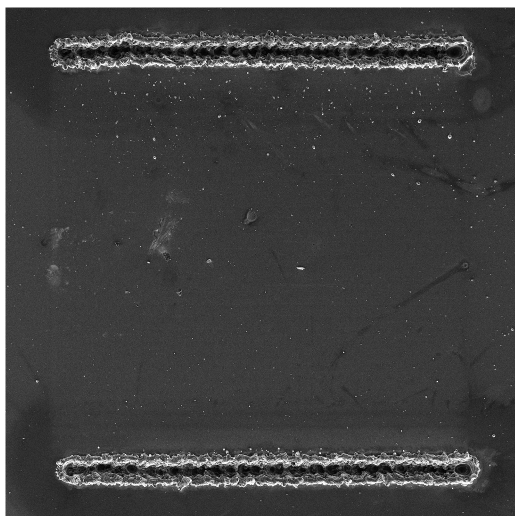

Figure 1. SEM image (energy 5 keV, magnification $378^{\times}$) of the Si:Mn sample surface with a 1×1 mm square area after PLA ($W = 1.3\,\mathrm{J/cm^2}$, 10 ppd). Top and bottom lines — are laser engraving traces.

Methods and materials

Double-side polished single-crystal Si (n-type phosphorus-doped silicon, resistivity $4-5\,\Omega\times\mathrm{cm}$) *n*-type, with crystal-lattice orientation (100) and $350\,\mu$m in thickness was used as initial samples. Before implantation, the Si plate was put into hydrofluoric acid (HF) to remove the surface oxide (SiO_2), then washed in distilled water and dried in compressed air. ILU-3 ion-beam accelerator was used for implantation of *n*-Si plate with singly charged Mn^+. Manganese chloride served as a substance for ion production. Ion energy Mn^+ was $E = 40$ keV. Ion dose (fluence) was $D = 1 \times 10^{16}\,\mathrm{ions/cm^2}$ at ion beam current density $j = 3\,\mu\mathrm{A/cm^2}$. Implantation was conducted with water cooling of a steel container with the exposed Si substrate and at normal incidence of Mn^+ beam. According to the calculations of Mn^+ paths in Si in SRIM software, the design ion path for 40 keV is equal to $R_p = 38$ nm at a profile width of 33 nm. According to the implantation dose and ion path data, the maximum concentration of Mn atoms in the distribution peak may achieve $2.8 \times 10^{21}\,\mathrm{cm^{-3}}$ (5.6 at.%).

Pulsed laser annealing of the implanted Si plate was carried out on HTF MARK laser system (Zelenograd, Russian Federation) using 120 ns laser pulses with a central wavelength of 1064 nm. The maximum pulse repetition rate of the system is 80 kHz and the maximum pulse energy is 1 mJ. Focusing and surface scanning by laser radiation were performed using a galvanometer double-mirror scanner equipped with F-θ-lens with a focal distance of 160 mm. The focused Gaussian laser beam diameter was about $50\,\mu$m at $1/e^2$ of its maximum intensity. The laser annealing experiments were carried out at normal beam incidence in sulfur hexafluoride gas atmosphere (SF_6) supplied to an insulated chamber at 2×10^5 Pa to displace atmospheric gases and steam. For the experiments using laser-beam raster scanning with scanline spacing about $30\,\mu$m, 1×1 mm square areas were treated (Figure 1). To achieve the best crystallinity of silicon plates, laser energy density acting on the surface was varied from $W = 1.0\,\mathrm{J/cm^2}$ to $2.0\,\mathrm{J/cm^2}$ in increments of $0.1\,\mathrm{J/cm^2}$. The pulses per dot were also varied -10, 20 and 100 ppd. While the energy density was varied by pulse energy variation, the pulses per dot were varied by varying scanning rate 100, 20, 10 mm/s for 10, 20 and 100 ppd, respectively. The pulse repetition rate was fixed at 20 kHz.

The crystal properties of the samples were studied by the 3D scanning Raman scattering spectroscopy method using Confotec 350 spectromicroscope (SOL instruments, Belarus) at an excitation wavelength of 532 nm with spectral resolution of $0.5\,\mathrm{cm^{-1}}$.

For surface topography and chemical analysis, Tescan Vega scanning electron microscopy (SEM) equipment (Czech Republic) was used. Xplore EDX detector made by Oxford Instruments (UK) was used for energy-dispersive X-ray spectroscopy.

IR transmission and reflection spectra in the wavenumber range from 700 to $1300\,\mathrm{cm^{-1}}$ (wavelengths — from 14.3 to $7.7\,\mu$m) were measured at room temperature using FT-805 infrared Fourier spectrometer (Simex, Russia) with a spectral resolution of $0.5\,\mathrm{cm^{-1}}$. Sample absorption was later calculated using the following equation

$$A = 100\% - R - T,$$

where A is the absorption, R is the reflection and T is the transmission.

Findings and discussion

Structure of the implanted and laser-annealed samples was examined using the Raman spectroscopy method. Each laser-treated area was examined by measuring Raman spectrum in 100 points in a small area of $100 \times 100\,\mu$m. Then, arithmetic mean of 100 values of recorded Raman spectra was calculated for integral assessment of crystallinity of the total treated surface area.

Figure 2 shows the Raman spectra for the origin single-crystal Si sample and for Mn^+ implanted Si samples before and after PLA with optimized energy density $W = 1.3\,\mathrm{J/cm^2}$ at ppd = 10. This energy density was chosen considering the best symmetry of the base peak of crystalline Si ($521\,\mathrm{cm^{-1}}$). The Raman spectrum of the origin *n*-Si(100) substrate has phonon peaks at 305, 521 and $955\,\mathrm{cm^{-1}}$. The Raman spectrum after ion implantation has peaks at 170, 305 and $521\,\mathrm{cm^{-1}}$ and an „arm" at $480\,\mathrm{cm^{-1}}$. Peaks at 170 and $480\,\mathrm{cm^{-1}}$ are assigned to the amorphous Si phase on the surface and peaks at 305 and $521\,\mathrm{cm^{-1}}$ are induced by underlying single-crystal substrate layers because the green laser light (532 nm) used for Raman signal excitation penetrates the silicon to a depth of

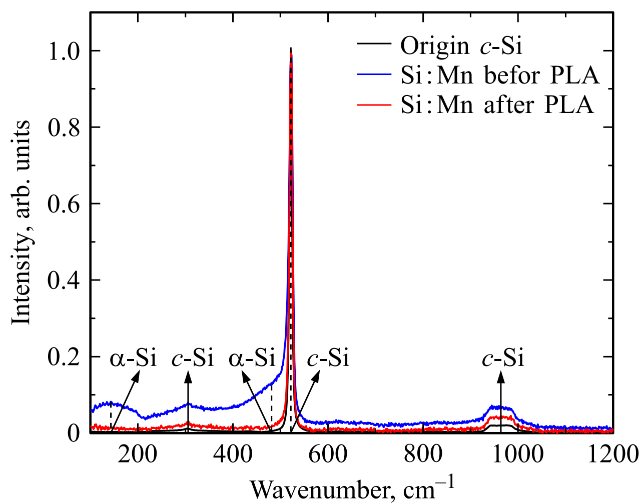

Figure 2. Raman spectrum for the origin single-crystal Si sample (black line) and for implanted Si:Mn samples before PLA (blue line) and after PLA (red line).

≈ 1 μm. Laser processing of the implanted layer with melt achievement results in the disappearance of amorphous Si phase traces and the Raman spectrum of the sample in this case closely resembled the origin crystal spectrum.

Figure 1 shows a SEM image of the Si:Mn sample surface with the test area after PLA. Two lines on the top and bottom were engraved by laser before for easy orientation during examination. The treated 1×1 mm square area is between the two lines. The image of the laser-affected area exhibits slight roughness. The same contrast in the areas on the image before and after annealing shows that these areas have similar atomic composition. Also, the image shows individual melt drops and contamination that may be removed by more careful cleaning of silicon, for example by the RCA technique [12]. The table shows atom concentrations of the main chemical elements (silicon, manganese and oxygen) for the samples before and after PLA. The surface was examined by the EDX method with irradiation by an electron beam at an accelerating voltage of 10 keV. Therefore, the approximate depth of electron-beam probing was about 600 nm [13]. No significant changes in the concentration of main chemical elements were found after PLA, only a slight redistribution at a level of percent proportions occurred, which corresponds to the SEM data (Figure 1). A relatively low content of oxygen at a level of atom percent units indicates the presence of a thin silicon oxide layer on the sample surface. In addition, it should be noted that the oxygen concentration remained almost unchanged after PLA in the inert gas atmosphere, which differs from the expected increase during laser processing in air [14].

Figure 3 shows the IR absorption spectra in a wavenumber range from 700 to 1300 cm^{-1} for the initial single crystal silicon sample and for implanted Si:Mn samples before and after PLA. Dashed lines show the main IR absorption band positions in silicon compounds [15,16]. Si-O-Si-absorption bands are clearly seen at 820 cm^{-1}, 970 cm^{-1} and 1108 cm^{-1}. Moreover, at 740 cm^{-1}, an absorption peak for metasilicate (SiO_3) is seen. Also, there is a hydroxide peak (Si-OH) at 880 cm^{-1}. The Figure shows that the absorption level of the origin sample in the examined spectral region is 10−25%. After implantation, the absorption level in the Si:Mn sample will grow a little, probably, due to the radiation-induced defects. After PLA, the absorption level will considerable grow up to 40%. This growth is probably caused by formation of an impurity band due to high concentration of Mn atoms (more than 2×10^{21} cm^{-3}) after implantation and PLA. Also, the effect of high carrier (hole) concentration on the absorption level cannot be ruled out [17], but requires further electrophysical measurements by the Hall effect method. Thus, optimized PLA of Mn^+ implanted silicon in SF_6 also helps remove Si amorphization effectively, avoid penetration of foreign sulphur and fluorine impurities, and considerably increase the middle-IR absorption of the sample due to formation of the impurity band.

Concentration of main chemical elements of the Si:Mn samples before and after PLA

Element	before PLA, at.%	after PLA, at.%
Si	97.14	97.09
Mn	1.60	1.5
O	1.25	1.36

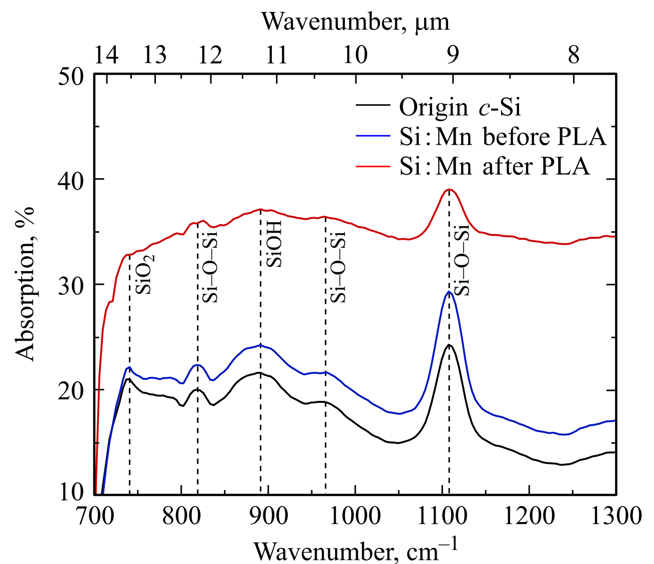

Figure 3. IR absorption spectrum for the origin single-crystal Si sample (black line) and for implanted Si:Mn samples before PLA (blue line) and after PLA (red line).

Conclusion

The study selected the appropriate PLA conditions for silicon plates hyperdoped with manganese atoms using ion implantation to ensure the best crystallinity of the samples. The appropriate energy density of laser pulses was equal to 1.3 J/cm^2, and the number of pulses per dot was 10 ppd.

After PLA, the Raman spectrum suggested a sudden decrease in the amorphous component of the material and increase in crystallinity. Examination of SEM images and review of EDX data showed a slight change in the concentration of the main chemical elements. The main absorption bands of silicon oxides and hydroxides were identified on the IR absorption spectra, and assumptions on the causes behind the increase in IR absorption after PLA were made.

Funding

Experiments for ion implantation of silicon with manganese ions were conducted under the KPTI public job-order. Experiments for pulsed laser annealing and further silicon characterization were carried out under Agreement № 075-15-2023-612 with the Ministry of Science and Higher Education of the Russian Federation.

Conflict of interest

The authors declare that they have no conflict of interest.

References

[1] C. Li, J.-H. Zhao, Z.-G. Chen. J. Alloys Compd., **883**, 160765 (2021). DOI: 10.1016/j.jallcom.2021.160765
[2] S. Kudryashov, K. Boldyrev, A. Nastulyavichus, D. Prikhod'ko, S. Tarelkin, D. Kirilenko, P. Brunkov, A. Shakhmin, K. Khamidullin, G. Krasin, M. Kovalev. Opt. Mater. Express, **11** (11), 3792 (2021). DOI: 10.1364/OME.438023
[3] S. Kudryashov, A. Nastulyavichus, G. Krasin, K. Khamidullin, K.Boldyrev, D. Kirilenko, A. Yachmenev, D. Ponomarev, G. Komandin, S. Lebedev, D. Prikhod'ko, M. Kovalev. Opt. Laser Technol., **158**, 108873 (2023). DOI: 10.1016/j.optlastec.2022.108873
[4] M. Kovalev, A. Nastulyavichus, I. Podlesnykh, N. Stsepuro, V. Pryakhina, E. Greshnyakov, A. Serdobintsev, I. Gritsenko, R. Khmelnitskii, S. Kudryashov. Materials, **16** (12), 4439 (2023). DOI: 10.3390/ma16124439
[5] V.N. Abakumov, V.I. Perel', I.N. Yassievich. *Bezyzluchatel'naya rekombinatsiya v poluprovodnikakh* (Isd. FTi im. Ioffe RAN, 1997) (in Russian).
[6] M. Bolduc, C. Awo-Affouda, A. Stollenwerk, M.B. Huang, F.G. Ramos, G. Agnello, V.P. LaBella. Phys. Rev. B, **71** (3), 033302 (2005). DOI: 10.1103/PhysRevB.71.033302
[7] L. Li, D. Bürger, A. Shalimov, G.J. Kovacs, H. Schmidt, S. Zhou. J. Phys. D: Appl. Phys., **51** (16), 165304 (2018). DOI: 10.1088/1361-6463/aab5a6
[8] N. Peng, C. Jeynes, M.J. Bailey, D. Adikaari, V. Stolojan, R.P. Webb. Nucl. Instrum. Methods Phys. Res. B, **267** (8–9), 1623-1625 (2009). DOI: 10.1016/j.nimb.2009.01.065
[9] C. Awo-Affouda, M. Bolduc, V.P. LaBella. J. Vac. Sci. Technol. A, **25** (4), 976–979 (2007). DOI: 10.1116/1.2713117
[10] M. Naito, R. Yamada, N. Machida, Y. Koshiba, A. Sugimura, T. Aoki, I. Umezu. Nucl. Instrum. Methods Phys. Res. B, **365**, 110–113 (2015). DOI: 10.1016/j.nimb.2015.07.073
[11] S. Zhou, K. Potzger, G. Zhang, A. Mcklich, F. Eichhorn, N. Schell, R. Grötzschel, B. Schmidt, W. Skorupa, M. Helm, J. Fassbender, D. Geiger. Phys. Rev. B, **75** (8), 085203 (2007). DOI: 10.1103/PhysRevB.75.085203
[12] W. Kern. J. Electrochem. Soc., **137**, 1887 (1990). DOI: 10.1149/1.2086825
[13] L. Zarraoa, M.U. González, Á.S. Paulo. J. Sci. Rep., **9**, 16263 (2019). DOI: 10.1038/s41598-019-52690-9
[14] M. Kovalev, I. Podlesnykh, A. Nastulyavichus, N. Stsepuro, I. Mushkarina, P. Platonov, E. Terukov, S. Abolmasov, A. Dunaev, A. Akhmatkhanov, V. Shur, S. Kudryshov. Materials, **16** (6), 2350 (2023). DOI: 10.3390/ma16062350
[15] T. OH, C.K. Choi. J. Korean Phys. Soc., **56** (4), 1150–1155 (2010). DOI: 10.3938/jkps.56.1150
[16] B. Arkles, G.L. Larson. *Silicon Compounds: Silanes & Silicones*, 3rd ed. (Gelest Inc., Morrisville, PA 19067, 2013).
[17] L. Jastrzebski, J. Lagowski, H.C. Gatos. J. Electrochem. Soc., **126** (2), 260 (1979). DOI: 10.1149/1.2129017

Translated by E.Ilinskaya